Indian Geotechnical Journal, 34 (2), 2004

Investigations into Shear Band Formation in Clay

Siddhartha Sengupta and Aniruddha Sengupta

Introduction

Some soils exhibit both in laboratory and in field situations, strain accumulations along well-defined narrow zones. These are called shear bands. A shear band may also be defined as a thin material layer undergoing simple shear Particular examples can be found in brittle geomaterials such as concrete and rocks, where progressive damage produces strain softening, or in some soils as for instance in the case of landslides or foundation failure. The formation of shear bands is influenced by one or more of the following factors – porosity of the medium, inherent anisotropy of the medium, grain size and grain shape, level of effective isotropic stress (Papamichos and Vardoulakis, 1995). Study of strain localization is not new. Many researchers have attempted to capture strain localization experimentally and numerically. Some of the important research works are by Rudnicki and Rice (1975); Vardoulakis (1980, 1985); Arthur and Assadi (1977); Vardoulakis, Goldscheider and Gudehus (1978); Prevost (1984); Vardoulakis and Graf (1985); Bolton (1986); Lade and Nelson (1987); Mühlhaus and Vardoulakis (1987); Peters, Lade and Bro (1988); Drescher et al. (1990); Vermeer (1990); Alsiny, Vardoulakis and Drescher (1992); Finno and Rhee (1993); Saada, Bianchini and Liang (1994); Chu, Lo and Lee (1993); Alshibli and Sture (2000).

But only a handful of researches can be cited those who have compared formation and propagation of shear bands in clay as observed in the laboratory experiments and in the numerical analyses. Most of the laboratory

* Research Scholar, Department of Civil Engineering, Indian Institute of Technology Kharagpur, Pin – 721302, India.

† Assistant Professor, Department of Civil Engineering, Indian Institute of Technology Kharagpur, Pin – 721302, India. E-mail: sengupta@civil.iitkgp.ernet.in

experiments on soils are performed under conventional triaxial (axisymmetric) conditions for the purpose of evaluating their behavior and material properties. However, present investigations have been carried out under plane strain conditions since many geotechnical problems like, embankment failure, landslides, bearing capacity failure of shallow foundations, etc., are usually idealized as plane strain problems. The strength and deformation characteristics of soils under plane strain are considerably different from those observed in triaxial tests. A dense and homogeneous sand tested in plane strain has higher strength and smaller strains at failure than when tested under triaxial condition at the same confining pressure as observed by Lee (1970) and Marachi et al. (1981). The failure in plane strain condition occurs along well defined shear plane(s), whereas, in axisymmetric condition, either localized shear plane or bulging failure occur depending on the density and the confining pressure (Lee, 1970; Peters et al., 1988). Thus, use of strength parameters from triaxial tests will in most cases lead to a conservative design, but soils loaded in plane strain is more susceptible to instability or bifurcation where sudden failure can occur much sooner than that is typically observed in triaxial condition.

In the present study, a plane strain testing device is developed to capture and study shear band formations in clayey soil. Kaolinite has been used in lieu of natural clay. A strain controlled finite element algorithm is developed to predict the propagation of shear bands and their patterns numerically. Nonuniformity of the deformations has been observed after attaining the peak stress, in all the cases. Typical results and findings concerning the evolution of shear bands and their behavior with the progress of the tests are discussed in detail. A comparative study between the experimental data and its numerical simulation is presented.

Review of Literature

The framework for analyzing the onset of shear bands started with the work of Hadamard (1903) for elastic solids. Later, the plastic flow and fracture in solids were investigated by Thomas (1961). In 1962, a general theoretical work on localization was done by Hill for elasto-plastic solids. The above three works are the earliest and the most important works on localization.

Later, Rice (1977), Rudnicki and Rice (1975), Prevost (1984), Vermeer and De Borst (1986), Needleman and Tvergaard (1983), Lade and Nelson (1987), Finno et al. (1997) and others have investigated the strain localization or shear band formation in sands theoretically using non-associative flow rules and weak elements, etc., in finite element analysis.

Vardoulakis et al. (1978), Vardoulakis (1980), Mühlhaus and Vardoulakis

(1987), Saada et al. (1994), Drescher et al. (1990), Vermeer (1990), Lade et al. (1987), Desrues et al. (1996), Chu et al. (1996), Arthur et al. (1977), Scarpelli and Wood (1982), Peters et al. (1982), Alshibli and Sture (2000) have studied strain localization and its orientation in soils in laboratory tests. X-rays, radiography, stereophotogammetry and tomography were utilized to track the formation of shear bands during the tests. Most of these tests were done on dry sands. The major findings are that shear bands are initiated more easily under plane strain than under axisymmetric condition. In all cases bands are formed after peak stress is reached, that is, in the hardening (in tensile tests) / softening (in compression tests) regime. The soil is found to deform at constant volume in a persistent band. The width of the bands found to be dependent on mean grain size. The shear band inclination is a geometrical mean of classical Coulomb and Roscoe solutions depending on the mean grain size. That is, inclination of the shear bands falls between the limits of $\theta_R = 45° + \Psi/2$ (Roscoe type) and $\theta_C = 45° + \phi/2$ (Coulomb type), where Ψ is the angle of dilatancy and ϕ is the angle of internal friction respectively.

Most of the above works are done on dry sand. The study of strain localization in saturated clay is quite rare. Morgenstern and Tchalenko (1967) studied the behavior of thin sections of carbowax-impregnated clay in a direct shear device. They showed that the kinematic restraint imposed by the testing configuration has a marked influence on the shear bands. Balusubramanium (1976) used X-rays to study the pattern of deformation in clays. He found the strains to be uniform up to 75% of the peak value. Finno and Rhee (1993) studied consolidation, pre and post-peak shearing responses of Chicago clay in biaxial compression device. They found that nonuniformity of deformations in clays begins after the peak stress has been attained during undrained plane strain compression. Saada et al. (1994) also reported a study on the localizations in saturated clays under combined stresses. Lizcaño et al. (1997) conducted a series of plane strain tests on saturated, anisotropically consolidated kaolinite to investigate shear band formation and shear band orientation. They reported that the nonuniform deformation always occurs in the vicinity of the maximum deviatoric stress.

Conditions for Orientation of Shear Band

According to Rice (1977), for the stress state σ_{ij} and the velocity gradient field $V_{k,l}$, if the constitutive rate relation is imagined to have the form:

$$\sigma_{ij} = C_{ijkl} \cdot V_{k,l} \tag{1}$$

The critical condition for localization on a plane is first met when

$$\det\left(n_i \cdot C_{ijkl} \cdot n_l\right) = 0 \tag{2}$$

here, C_{ijkl} is stiffness matrix, n_i and n_l are normals. The above condition has been simplified by Bardet and Mortazavi (1987) for a plate subjected to plane strain with uniform prescribed displacements where the Von Mises material model is used. According to them, the orientation of shear band can be determined as:

$$\alpha = \tan^{-1}\left[\pm\left\{1 \pm \sqrt{-\beta(2+\beta)}\right\}^{1/2} \Big/ (1+\beta)^{1/2}\right] \tag{3}$$

where β = H/2G,

H = plastic hardening modulus,

G = shear modulus, and

α = orientation of the shear band.

In conformity with the notation for systems of partial differential equations, elliptic, parabolic, or hyperbolic regimes can be identified depending upon whether there are no, two or four real values of the orientation (α) of shear bands,

Elliptic : $\beta > 0$ or $\beta < -1$ (Bifurcation excluded);

Parabolic : $\beta = 0$, or $\beta = -1$;

Hyperbolic : $0 > \beta > -1$ (4)

Peters, Lade and Bro (1988) discussed the conditions associated with shear banding in great details. They have aligned the co-ordinate system x_1 - x_2 - x_3 (Fig.1) in such a way that the x_1 axis is parallel to the shear band, the x_2 axis is perpendicular to the shear band, and x_3 lies within the plane of the shear band, but is perpendicular to the plane of sliding. It can be then shown that x_3 corresponds to intermediate principal stress σ_2. If the increments of displacements along and across the band are denoted by u_1 and u_2 respectively, then the kinematic conditions for shear banding can be expressed in terms of the incremental displacement gradients as follows:

$$\partial u_1/\partial x_2 = g_1(x_2) \tag{5}$$

$$\partial u_2/\partial x_2 = g_2(x_2) \tag{6}$$

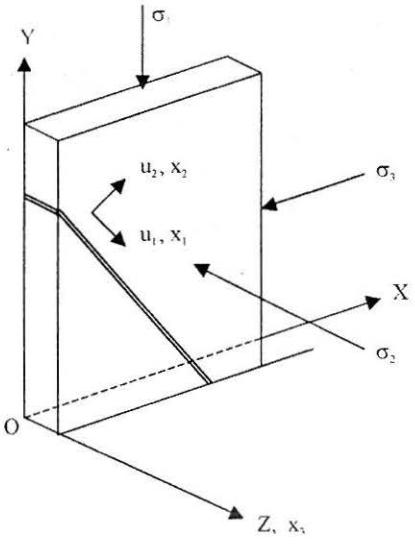

FIGURE 1 : Formation of Shear Band in Soil

$$\partial u_1/\partial x_1 = 0 \tag{7}$$

$$\partial u_2/\partial x_1 = 0 \tag{8}$$

where, g_1 and g_2 are arbitrary functions that depend only on x_2. These relationships define the condition whereby all displacement gradients occur across the band (x_2 direction). Separation may occur as a result of dilation of the soil within the band but there is no stretching along the band (x_1 and x_3 directions).

In addition to the kinematic conditions, equlibrium must be maintained as localization occurs. The stress changes inside of the band must be restricted as follows:

$$\Delta\sigma_{22} = \Delta\sigma_{12} = \Delta\sigma_{23} = 0 \tag{9}$$

Material Properties of Kaolinite

A commercially available kaolinite is utilized for all the laboratory tests instead of natural clay. Its specific gravity is 2.68. The Liquid Limit, the Plastic Limit and the Plasticity Index of the kaolinite are 50%, 31% and 19%, respectively. The soil is classified as ML according to Unified Soil Classification. As per Indian code IS:1498-1970, the soil is classified as CI

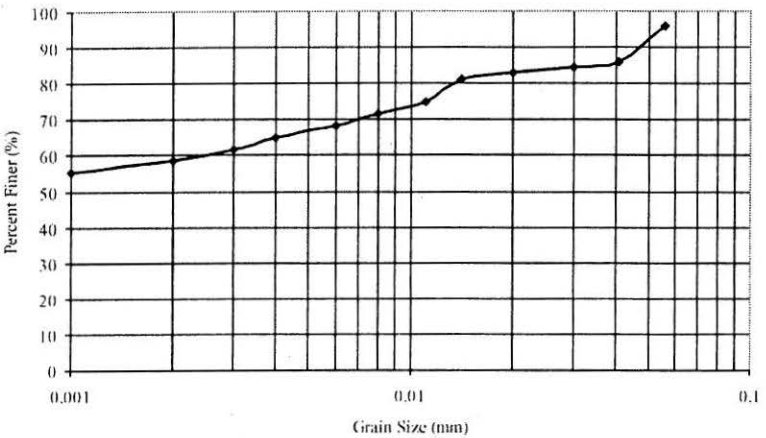

FIGURE 2 : Grain Size Distribution Curve of Kaolinite

material. The grain size distribution curve of the kaolinite is shown in Fig.2. The elastic and the hardening material parameters of the kaolinite are computed from the experimental stress-strain curves obtained from the undrained tests on the kaolinite under plane strain (biaxial) condition. In the numerical analyses, the stress-strain behavior of the kaolinite under undrained condition is idealized by extended Von Mises yield theory, that is, by a bilinear curve as can be seen in Fig.3. The initial straight-line represents the elastic portion of the experimental stress-strain curve. The elastic shear modulus (2G) is obtained as the slope of this initial straight-line. The value

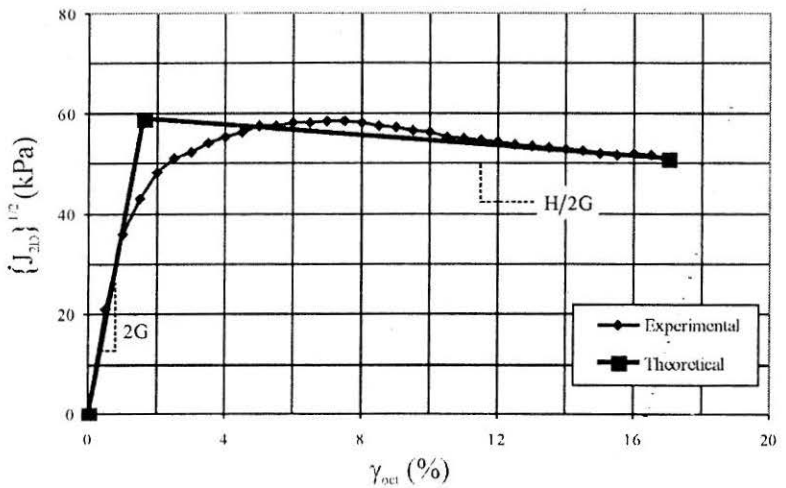

FIGURE 3 : Stress-Strain Curve from Biaxial Test No.1

TABLE 1 : Material Parameters

Test No.	Density (g/cc)	Moisture Content (%)	E (kPa)	H/2G
1.	1.82	43.43	3687.5	−0.0207
2.	1.75	51.56	2828.6	−0.0018
3.	1.61	53.63	2600	−0.0080
4.	1.58	42.65	1866.7	−0.0079

of Poisson's ratio (ν) is taken as 0.49 for all the undrained analyses. The straight-line, which represents the later portion of the experimental stress-strain curve, models the material strain softening (or strain hardening) observed in the laboratory experiment. The slope (H) of this straight-line, when normalized by dividing it by shear modulus (2G), represents the hardening modulus (H/2G) of the numerical model. The stress at the

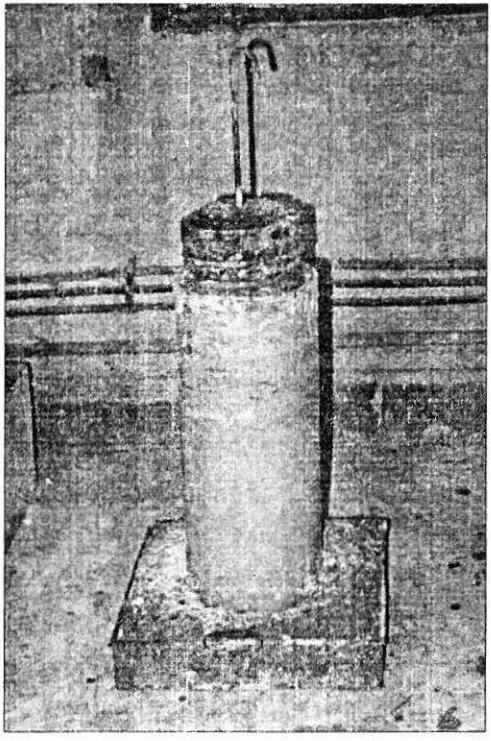

FIGURE 4 : Preparation of Samples

junction of the above two straight lines corresponds to the idealized yield stress (κ) of the soil. Figure 3 shows the experimental stress-strain curve from Test 1 and the corresponding idealized stress-strain curve used in the numerical analyses. Table 1 summarizes the material properties of the kaolinite as obtained from four of the laboratory experiments performed.

Preparation of Samples

The soil samples are prepared in a circular slurry tank of diameter 450 mm. The tank with both ends open is placed in a sand bath to facilitate drainage of water through the bottom. A uniform slurry of kaolinite is prepared in the tank and it is allowed to consolidate under a uniform pressure of 8.5 kPa for 15 days to 30 days. The whole setup is shown in Fig.4. Fully consolidated and saturated soil samples are extruded from the middle of the tank (to ensure homogeneity) with the help of a rectangular split mould of 150 mm × 75 mm × 30 mm dimensions.

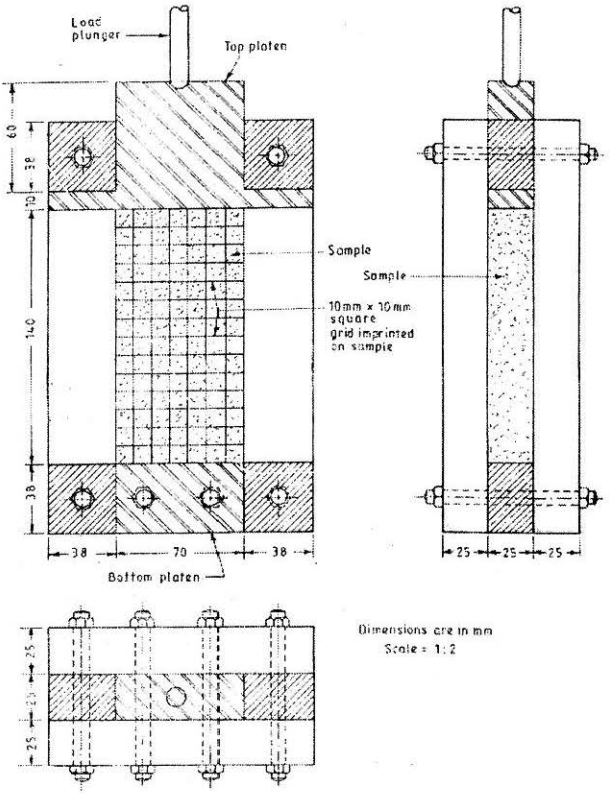

FIGURE 5 : Plane Strain Testing Cell

Laboratory Experimental Programme

The laboratory plane strain test cell is manufactured in-house. It consists of two perspex plates of 226 mm × 146 mm × 25 mm in size (Fig.5) bolted together with a 140 mm × 70 mm × 25 mm soil specimen sandwiched in between them. The bottom end platen is restrained from movement and the top end platen can slide smoothly in the vertical direction only between two fixed guides. The bottom of the top platen is considered to be rough. No attempt is made to smoothen the interface between the top platen and the soil sample.

Before the tests, square grids of 10 mm × 10 mm are imprinted on the soil samples so that deformations and locations of the shear bands within the soil sample can be visualized and measured with the progress of the tests. A template of 10 mm × 10 mm size grids is prepared. The grids are then imprinted on the clay samples by indelible ink. A stationary CCD camera is utilized to record the deformation of the grids with the progress of the axial strain. The average axial stress, deformations in axial and in both horizontal directions are measured with pressure transducer and LVDTs.

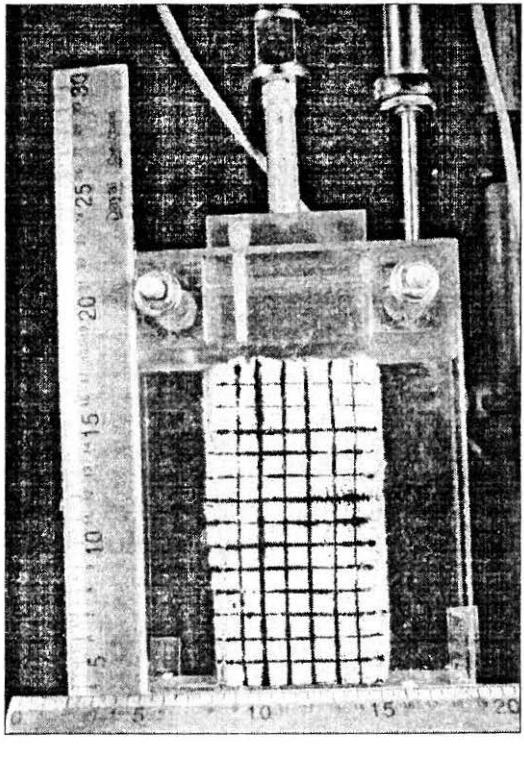

FIGURE 6 : Plane Strain Test Set-up

The inside walls of the perspex sheets are coated with oil to reduce friction between the soil sample and the cell walls. The whole plane strain device, with soil specimen in it, is mounted on a triaxial loading frame. Two measuring rulers (one in horizontal and another in vertical directions) are fixed to the device to accurately trace the coordinates of the deformed mesh at different stages of the experiment. The triaxial loading machine is strain controlled. The soil sample is compressed by lowering the top platen at a constant rate of 1.2 mm per minute (0.86% strain). Figure 6 shows the whole plane strain test setup. The average stress-strain behavior of the kaolinite sample from Test 1 is shown in Fig.3. Figure 7 shows the corresponding deformations of the soil sample at 4%, 7%, 10%, 13% and 15% axial strains. Figure 8 depicts the corresponding velocity vectors at 4%,

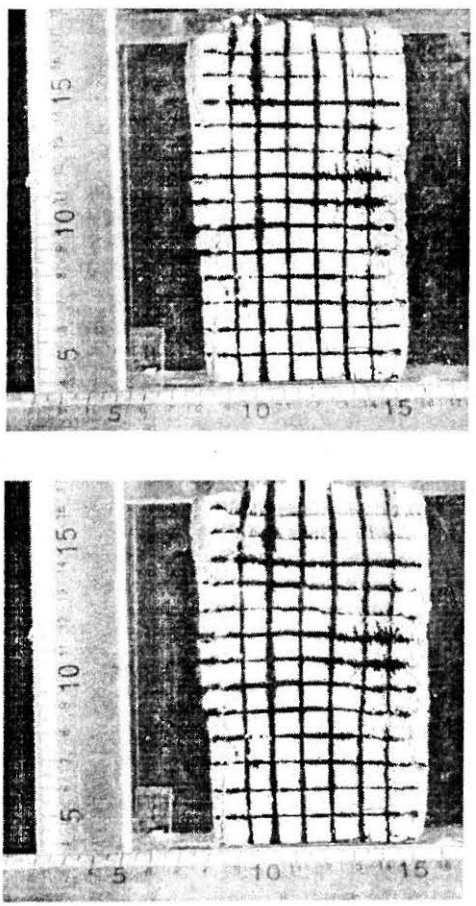

FIGURE 7 : Deformation of Soil Sample in Test 1 at (a) 4% Axial Strain; (b) 7% Axial

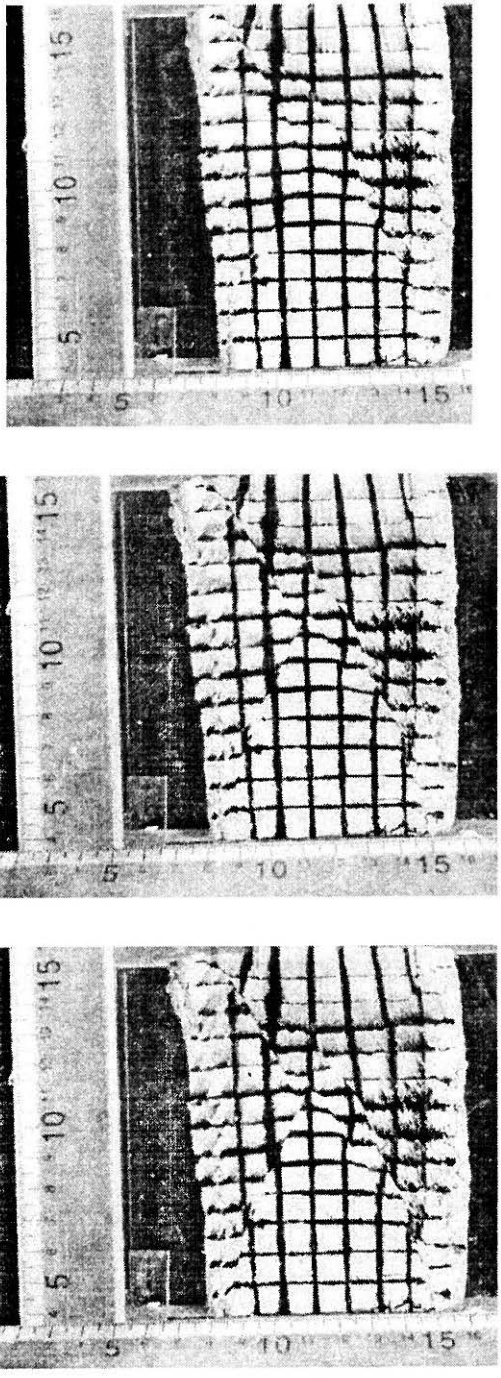

FIGURE 7 : Deformation of Soil Sample in Test 1 at (c) 10% Axial Strain; (d) 13% Axial Strain; (e) 15% Axial Strain

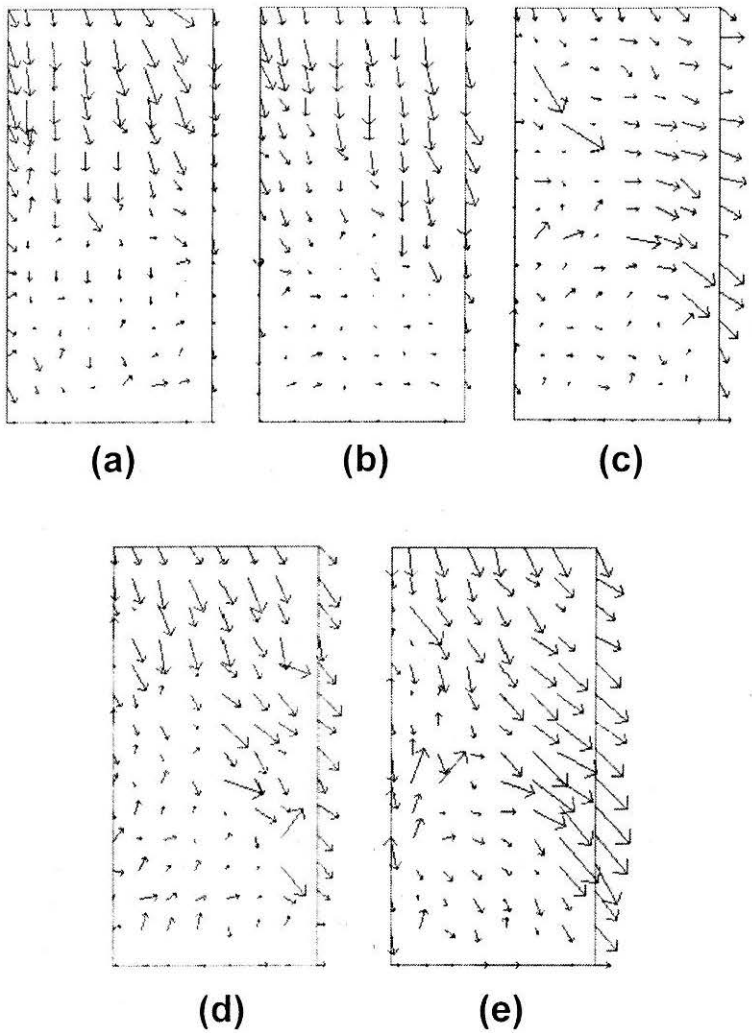

FIGURE 8 : Velocity Vectors for Test 1 at (a) 4% Axial Strain; (b) 7% Axial; (c) 10% Axial Strain; (d) 13% Axial Strain; (e) 15% Axial Strain

7%, 13% and 15% axial strains. The velocity vectors are computed from the digitized data of the deformed grids of the soil sample.

In all the four laboratory tests, shear bands initiate after the peak-stress is reached, that is, around 7% axial strain. At 7% strain only one shear band became prominent. At 10% axial strain, a conjugate band emerges. After 12% strain level, both the bands become very prominent. From the velocity vector plots, appearance of one single shear band can be seen, but the

TABLE 2 : Comparison of Numerical and Laboratory Test Results

Test No.	Inclination of Shear Band (degrees)			Width of Shear Band (mm)	
	Obtained from Experiment	Obtained from Present Numerical Analysis	Obtained from Eqn.3	Obtained from Experiment	Obtained from Present Numerical Analysis
1.	52	47	50.55	8.88	10.21
2.	48.75	42	46.69	10.76	11.07
3.	45	51	48.51	6.24	9.21
4.	41.25	39.5	48.49	6.18	7.83

emergence of the conjugate bands at later stage of the tests is not so obvious. This is mostly because of the crudeness of the imprinted mesh. A finer mesh is required to capture the formation of conjugate shear bands at higher strain levels. Table 2 summarizes the laboratory test results for all the four plane strain tests performed on kaolinite. The results indicate that the effect of specimen density and moisture content on strain localization is very prominent. As the specimen density increases, the shear bands emerge at comparatively lower values of axial strain.

Numerical Simulation

The objective of the numerical analyses is to simulate the plane strain tests numerically to see if the formation of shear bands and their patterns as observed in the laboratory tests can be also captured numerically. For this purpose, a plane strain, elasto-plastic finite element package has been developed in-house. The undrained behavior of kaolinite is modeled by a modified Von Mises yield theory. The classical Von Mises yield theory, originally developed for metals, models material behavior as a perfectly plastic material. The present theory includes strain dependent hardening (or softening) after the yield stress of the material is exceeded. In the π-plane (Fig.9), yield surfaces are represented by concentric circles. The material behavior is elastic as long as the value of second invariant of deviatoric stresses, $(J_{2D})^{1/2}$ does not exceed k, the size of the initial yield surface. The strain hardening/softening is dependent on the octahedral strain (γ_{oct}). When a material undergoes strain hardening, the subsequent yield surfaces are represented by concentric circles of sizes greater that κ. The strain softening behavior is represented by concentric circles of sizes smaller than the initial

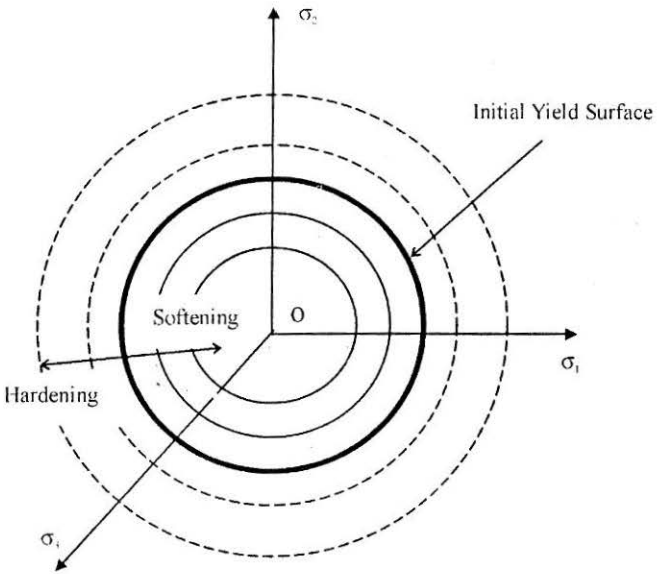

FIGURE 9 : Yield Surfaces in the Numerical Model

yield surface. In the $(J_{2D})^{1/2} - \gamma_{oct}$ space, the material behavior is represented by a bilinear curve as shown in Fig.3. The initial straight-line represents the elastic response of the material while the later straight-line represents the strain dependent hardening/softening behavior of the material. The material yield criterion assumed in the present analyses may be expressed as

$$F = F(\sigma, \varepsilon^P) = (J_{2D})^{1/2} - \left\{\kappa + H(\gamma_{oct})^P\right\} = 0 \qquad (10)$$

where J_{2D} = second invariant of deviatoric stresses

κ = size of initial yield surface

$(\gamma_{oct})^P$ = plastic octahedral shear strain, and

H = plastic hardening modulus

For plane strain condition, if the incremental stress and strain vectors are

$$d\sigma = \left\{d\sigma_{11}\ d\sigma_{22}\ d\tau_{12}\ d\sigma_{33}\right\}^T \qquad (11)$$

$$d\varepsilon = \left\{ d\varepsilon_{11}\ d\varepsilon_{22}\ d\gamma_{12} \right\}^{T} \tag{12}$$

The elastic and plastic stress-strain matrices can be shown as:

$$D^{e} = \frac{E}{(1+\nu)(1-2\nu)} \begin{pmatrix} 1-\nu & \nu & 0 \\ \nu & 1-\nu & 0 \\ 0 & 0 & (1-2\nu)/2 \\ \nu & \nu & 0 \end{pmatrix} \tag{13}$$

$$D^{P} = \frac{G}{1+\dfrac{H}{2G}\left(\dfrac{2}{\sqrt{6}}\right)} \begin{pmatrix} H_1H_1 & H_1H_2 & H_1H_3 \\ H_2H_1 & H_2H_2 & H_2H_3 \\ H_3H_1 & H_3H_2 & H_3H_3 \\ H_4H_1 & H_4H_2 & H_4H_3 \end{pmatrix} \tag{14}$$

where

$$H_1 = \left(J_{2D}\right)^{-1/2} S_{11} = \left(J_{2D}\right)^{-1/2} \left[\sigma_{11} - \left(\sigma_{11}+\sigma_{22}+\sigma_{33}\right)/3\right] \tag{15}$$

$$H_2 = \left(J_{2D}\right)^{-1/2} S_{22} = \left(J_{2D}\right)^{-1/2} \left[\sigma_{22} - \left(\sigma_{11}+\sigma_{22}+\sigma_{33}\right)/3\right] \tag{16}$$

$$H_3 = \left(J_{2D}\right)^{-1/2} S_{12} = \left(J_{2D}\right)^{-1/2} \tau_{12} \tag{17}$$

$$H_4 = \left(J_{2D}\right)^{-1/2} S_{33} = \left(J_{2D}\right)^{-1/2} \left[\sigma_{33} - \left(\sigma_{11}+\sigma_{22}+\sigma_{33}\right)/3\right] \tag{18}$$

In the finite element analyses, the soil specimen is discretized by 200 numbers of QM5 elements. The QM5 element is a five-noded constant strain quadrilateral element with a fifth interior node removed by static condensation. However, the stresses, strains and convergence are computed at the middle of this element to render greater stability of the algorithm.

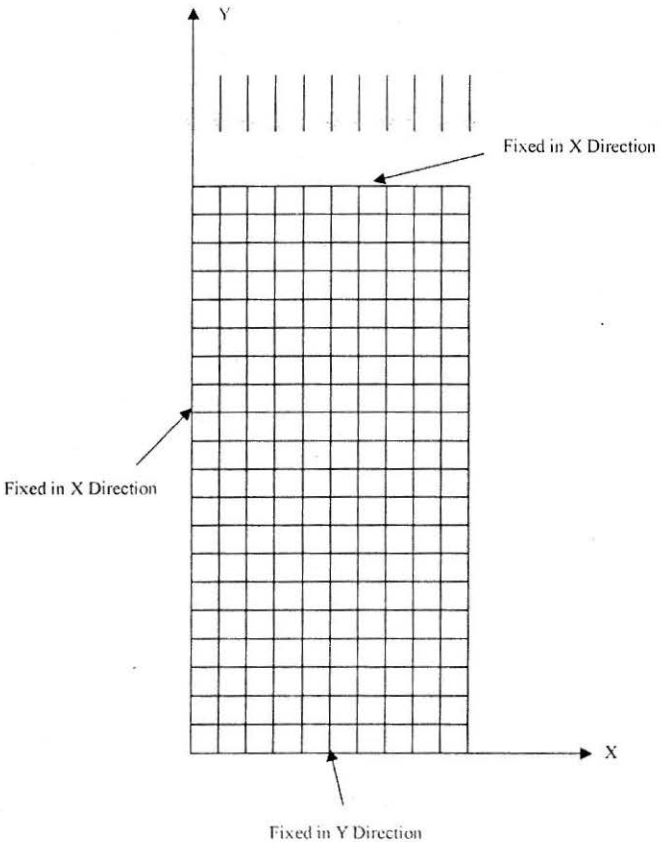

FIGURE 10 : Undeformed Mesh and Boundary Conditions Assumed in Numerical Modeling

The problem analyzed consisted of a rectangular soil sample under plane strain condition loaded at both ends by applying uniform prescribed vertical displacements. Assuming symmetry about both x- and y-axes, only one-fourth of the whole soil specimen has been considered for the present analyses. All the nodes along x-axis are restrained against movement in y-direction. Similarly, all the nodes along y-axis are fixed in x-direction. Horizontal displacements are constrained at the loaded ends. It is found that shear banding shall not form in the homogeneous stress conditions created by permitting free horizontal displacements at the loaded ends of the soil samples. By restraining the horizontal displacements at the loaded ends a sufficiently non-homogeneous strain is created to initiate shear banding even with uniform material properties. Figure 10 shows the undeformed mesh and the boundary conditions imposed for the finite element simulation of laboratory Test 1.

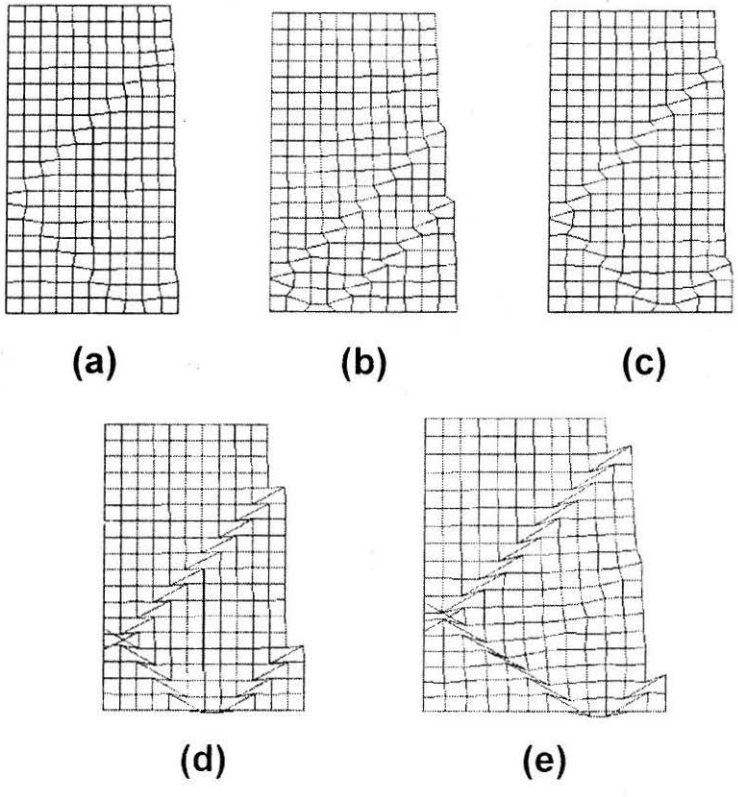

FIGURE 11 : Deformations with the Progress of Test 1 at (a) 4% Axial Strain; (b) 7% Axial; (c) 10% Axial Strain; (d) 13% Axial Strain; (e) 15% Axial Strain

Figures 11 and 12 display the results of the numerical simulation of laboratory Test 1. Figure 11 shows the deformation of the clay sample at 4%, 7%, 10%, 13% and 15% of axial strain. The corresponding velocity vectors have been shown in Fig.12. In the numerical simulation of Test 1, the shear bands first become visible at 4% strain, that is, well inside the strain softening regime. The shear bands become very prominent at 7% axial strain. From the velocity vector plots, the dynamics of the formation of shear bands can be visualized. The width of the bands becomes very prominent at 10% strain level. But with increasing strain level it becomes blurred most probably due to accumulation of numerical errors and increasing sensitivity of the algorithms. Table 2 summarizes the results of the numerical simulation of all the four laboratory plane strain tests.

The numerical analyses indicate that the location of the shear bands

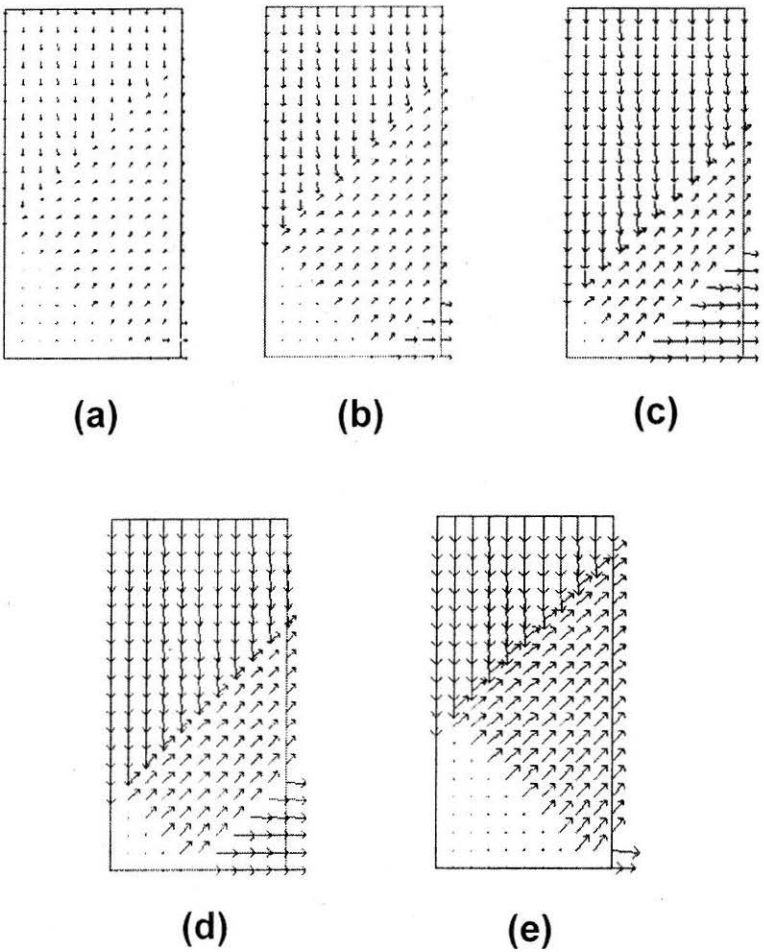

FIGURE 12 : Velocity Vectors Computed in Numerical Simulation of Test 1 at (a) 4% Axial Strain; (b) 7% Axial; (c) 10% Axial Strain; (d) 13% Axial Strain; (e) 15% Axial Strain

and the ease with which they appear are influenced by boundary conditions, mesh density and load steps. The thickness of the shear band is found to be dependent on the element size as it is directly related to the ease with which a disturbance will propagate from one element to another in a finite element analysis.

Comparisons between Experimental and Numerical Results

In the representative laboratory experiment shown in the present paper,

a single shear band first emerge at 7% axial strain, that is, when the peak-stress is reached. The conjugate band appears after 10 % axial strain, when the material is well into the softening regime. However, the width of the bands becomes a measurable quantity only after 13% strain level. In the corresponding numerical simulation, strain localizations initiate at 4% axial strain. The bands become very prominent with finite width, not before 10% axial strain is reached.

In the experiments, the shear banding is non-symmetrical. This is most probably due to unavoidable defects in the sample preparation and test setup. But numerically the bands appear to be always symmetrical due to initial assumption. But still the dynamics of the shear bands formation as observed in the experiments has been more or less successfully duplicated in the numerical simulations.

Table 2 compares the inclination angles of shear bands obtained in all the four experiments with those obtained from their corresponding numerical simulations. The shear band inclination angles are also obtained from Eqn.3 and compared with the corresponding numerical and experimental values. As can be seen from the table, the angle of inclination of shear bands obtained from the experiments, numerical analyses and from Eqn.3, lie within ± 10% of each other.

The widths of the shear bands as obtained from the laboratory tests and their corresponding numerical simulations are shown in Table 2.

Conclusions

In all the four laboratory experiments two conjugate shear bands initiated at different axial strain levels depending on the specimen density and moisture content. Softening becomes more prominent as the specimen density increases and strain localization occurs at earlier stage. In all plane strain compression tests, strain localization initiates only after the peak stress has been reached. However, the shear bands attain a finite width at a higher strain level (> 10%) when the material behavior is well within the softening regime. But with increasing strain level, it becomes blurred most probably due to accumulation of numerical errors and increasing sensitivity of the algorithms.

The developed finite element algorithm is fully capable of capturing the formation of shear bands in the numerical simulation of the laboratory tests. The inclination and width of the shear bands predicted in the numerical analyses are comparable with those observed in the laboratory tests.

The location of the shear bands and the ease with which they appear

in the numerical simulations are found to be influenced by boundary conditions, mesh density and load steps. The thickness of the shear band is found to be dependent on the element size as it is directly related to the ease with which a disturbance will propagate from one element to another in a finite element analysis.

References

ALSHIBLI, KHALID A. and STURE, S. (2000) : "Shear Band Formation in Plane Strain Experiments of Sands", *J. of Geotechnical and Geoenvironmental Engineering*, ASCE, Vol.126, No.6, pp.495-503.

ALSINY, A., VARDOULAKIS, I. and DRESCHER, A. (1992) : "Deformation Localization in Cavity Inflation Experiments on Dry Sand", *Geotechnique*, Vol.42, No.3, pp.395-410.

ARTHUR, J.R.F., DUNSTAN, T., AL-ANI, Q.A.J.L. and ASSADI, A. (1977) : "Plastic Deformation and Failure in Granular Media", *Geotechnique*, Vol.27, No.1, pp.53-74.

ARTHUR, J.R.F. and ASSADI, A. (1977) : "Ruptured Sand Sheared in Plane Strain", *Proc. IX ICSMFE*, Tokyo, Vol.1, pp.19-22.

BALASUBRAMANIUM, A.S. (1976) : "Local Strains and Displacement Patterns in Triaxial Specimens of Saturated Clay", *Soils Fdns.*, Vol.16, No.1, pp.101-114.

BARDET, J.P. and MORTAZAVI, S.M. (1987) : "Simulation of Shear Bands Formation in Overconsolidated Clay", *Proceedings of the Second International Conference on Constitutive Laws for Engineering Materials*, Tucson, Vol.2, pp.805-812.

BOLTON, M.D. (1986) : "The Strength and Dilatancy of Sands", *Geotechnique*, Vol.36, No.1, pp.65-78.

CHU, J., LO, S.C.R. and LEE, I.K. (1996) : "Strain Softening and Shear Band Formation of Sand in Multi-axial Testing", *Geotechnique*, Vol.46, No.1, pp.63-82.

CHU, J. and LO, S.C.R. (1993) : "On the Measurement of Critical State Parameters of Dense Granular Soils", *Geotechnical Testing Journal*, GTJODJ, Vol.16, No.1, pp.27-35.

DESRUES, J., CHAMBON, R., MOKNI, M. and MAZEROLLE, F. (1996) : "Void Ratio Evaluation Inside Shear Bands in Triaxial Sand Specimen Studied by Computed Tomography", *Geotechnique*, Vol.46, No.3, pp.529-546.

DRESCHER, A., VARDOULAKIS, I. and HAN, C. (1990) : "A Biaxial Apparatus for Testing Soils", *Geotechnical Testing Journal*, GTJODJ, Vol.13, No.3, pp.226-234.

FINNO, R.J. and RHEE, Y. (1993) : "Consolidation, Pre- and Post-Peak Shearing Responses from Internally Instrumented Biaxial Compression Device", *Geotechnical Testing Journal*, GTJODJ, Vol.16, No.4, pp.496-509.

FINNO, R.J., HARRIS, W.W., MOONEY, M.A. and VIGGIANI, G. (1997) : "Shear Bands in Plane Strain Compression of Loose Sand", *Geotechnique*, Vol.47. No.1, pp.149-165.

HADAMARD, J. (1903) : "Lecons sur la Propagation des Ondes et les Equations de l'Hydrodynamique", Paris, cited in Reference [10].

HILL, R. (1962) : "Acceleration Wave in Solids", *Journal of the Mechanics and Physics of Solids*, Vol.10, pp.1-16.

KO, H.Y. and DAVIDSON, L.W. (1973) : " Bearing Capacity of Footings in Plane Strain", *J. Soil Mech. and Found. Div.*, ASCE, 96(3), pp.901-923.

LADE, P.V. and NELSON, R.B. (1987) : "Modelling the Elastic Behaviour of Granular Materials", *Int. J. Num. Anal. Meth. Geomech.*, Vol.11, pp.521-542.

LADE, P.V., YAMAMURO, J.A. and SKYERS, B.D. (1996) : "Effects of Shear Band Formation in Triaxial Extension Tests", *Geotechnical Testing Journal*, GTJODJ, Vol.19, No.4, pp.398-410.

LEE, K.L. (1970) : "Comparison of Plane Strain and Triaxial Tests on Sand", *Journal of Soil Mechanics and Foundations Division, Proc. ASCE*, Vol.96, No.SM 3, pp.901-922.

LIZSCANO, A., VARDOULAKIS, I. and GOLDSCHEIDER, M. (1997) : "Biaxial Tests on Normally, Anisotropically Consolidated Clay", *Deformation and Progressive Failure in Geomechanics*, (Eds. A. Asaoka, T. Adachi and F. Oka). Pergamon, pp.223-228.

MARACHI, N., DUNCAN, J., CHAN, C. and SEED, H. (1981) : "Plane-Strain Testing of Sand", *Laboratory Shear Strength of Soils*, ASTM STP 740, (Eds. R.N. Yong and F. C. Townsend), ASTM, West Conshohocken, Pa., pp.294-302.

MORGENSTERN, N.R. and TCHALENKO, J.S. (1967) : " Microscopic Structures in Kaolin subjected to Direct Shear", *Geotechnique*, Vol.17, pp.309-327.

MÜHLHAUS, H.B. and VARDOULAKIS, I. (1987) : "The Thickness of Shear Bands in Granular Materials", *Geotechnique*, Vol.37, No.3, pp.271-283.

NEEDLEMAN, A. and TVERGAARD, V. (1983) : "Finite Element Analysis of Localization in Plasticity", *Finite Elements: Special Problems in Solid Mechanics*, Vol.5, Eds. J.T. Oden, and G.F. Carey, Prentice-Hall, Inc., New Jersey, pp.94-157.

PAPAMICHOS, E. and VARDOULAKIS, I. (1995) : "Shear Band Formation in Sand according to Non-Coaxial Plasticity Model", *Geotechnique*, Vol.45, No.GT11, pp.1215-1228.

PETERS, J.F., LADE, P.V. and BRO, A. (1988) : "Shear Band Formation in Triaxial and Plane Strain Tests", *Advanced Triaxial Testing of Soil and Rock*, ASTM STP 977, Eds. R. Donaghe, R. Chaney and M. Silver, pp.604 -627.

PREVOST, J.H. (1984) : "Localization of Deformations in Elastic-Plastic Solids", *Int. J. Num. Anal. Meth. Geomech.*, Vol.8, pp.187-196.

RICE, J.R. (1977) : "The Localization of Plastic Deformation in Theoretical and Applied Mechanics", *Proc. 14th Int. Cong. Theo. Appl. Mech.*, Ed. W.T. Koiter, North-Holland Inc., Amsterdam, pp.207-220.

RUDNICKI, J.W. and RICE, J.R. (1975) : "Conditions of the Localization of Deformation in Pressure-Sensitive Dilatant Materials", *J. Mech. Phys. Solids*, Vol.23, pp.371-394.

SAADA, A.S., BIANCHINI, G.F. and LIANG, L. (1994) : "Cracks, Bifurcation and Shear Bands Propagation in Saturated Clays", *Geotechnique*, Vol.44, No.1, pp.35-64.

SCARPELLI, G. and WOOD, D.M. (1982) : "Experimental Observations of Shear Band Pattern in Direct Shear Tests", *Proc. IUTAM Conf. Deformation and Failure of Granular Materials*, Delft, pp.473-484.

THOMAS, T.Y. (1961) : *Plastic Flow and Fracture in Solids*, Academic Press, New York.

VARDOULAKIS, I. (1980) : "Shear Band Inclination and Shear Modulus of Sand in Biaxial Tests", *Int. J. Num. Anal. Meth. Geomech.*, Vol.4, pp.103-119.

VARDOULAKIS, I. (1985) : "Stability and Bifurcation of Undrained, Plane Rectilinear Deformations on Water-Saturated Granular Soils", *Int. J. Num. Anal. Meth. Geomech.*, Vol.9, pp.399-414.

VARDOULAKIS, I. and GOLDSCHEIDER, M. (1981) : "Biaxial Apparatus for Testing Shear Bands in Soils", *Proc. X ICSMFE,* Stockholm, Vol.1, pp.819-824.

VARDOULAKIS, I., GOLDSCHEIDER, M. and GUDEHUS, G. (1978) : "Formation of Shear Bands in Sand Bodies as a Bifurcation Problem", *Int. J. Num. Anal. Meth. Geomech.*, Vol.2, pp.99-128.

VARDOULAKIS, I. and GRAF, B. (1985) : "Calibration of Constitutive Models for Granular Materials using Data from Biaxial Experiments", *Geotechnique,* London, Vol.35, No.3, pp.299-317.

VERMEER, P.A. (1990) : "The Orientation of Shear Bands in Biaxial Tests", *Geotechnique*, Vol.40, No.2, pp.223-236 .

VERMEER, P.A. and DE BORST, R. (1986) : "Non-Associated Plasticity for Soils, Concrete and Rock", *Heron*, Vol.29, No.3, pp.1-64.

Notations

C_{ijkl}	=	Stiffness Matrix
D^e	=	Elastic stress-strain matrix
D^p	=	Plastic stress-strain matrix
E	=	Young's modulus
G	=	Shear modulus
H	=	Plastic hardening modulus
$(J_{2D})^{1/2}$	=	Second invariant of deviatoric stress
κ	=	Size of initial yield surface
n_i, n_l	=	Direction of normals
u_1, u_2	=	Increments of displacements along and across shear band

$V_{k,l}$	=	Velocity gradient field
σ_1	=	Major principal stress
σ_2	=	Intermediate principal stress
σ_3	=	Minor principal stress
σ_{ij}	=	Stress state
$\Delta\sigma_{22}$, $\Delta\sigma_{12}$, $\Delta\sigma_{23}$	=	Change in stresses inside the shear band
θ_R	=	Inclination of shear band (Roscoe Type)
θ_C	=	Inclination of shear band (Coulomb Type)
ν	=	Poisson' ratio
Ψ	=	Angle of dilatancy
ϕ	=	Angle of Internal friction
γ_{oct}	=	Octahedral shear strain
$(\gamma_{oct})^P$	=	Plastic octahedral shear strain